CEAS Aeronautical Journal
https://doi.org/10.1007/s13272-022-00583-5

ORIGINAL PAPER

Multirotor electric aerial vehicle model identification with flight data with corrections to physics-based models

Robert Niemiec[1] · **Christina Ivler**[2] · **Farhan Gandhi**[1] · **Frank Sanders**[3]

Received: 9 September 2021 / Revised: 24 February 2022 / Accepted: 31 March 2022

Abstract
Developing standard, well-vetted methods for modeling and simulation, prediction of flying/handling qualities, and control system design is critical for improving safety and quality control of multirotor electric aerial vehicles. This paper explores two methods for modeling the dynamics of a small (56 cm, 1.56 kg) hexacopter at hover and forward flight. The first modeling method was system identification from flight data, the second method was a physics-based blade element model with 10 state Peter-He inflow. Evaluation of the fidelity for both the system-identification and physics-based models was completed by comparison to flight data at hover and forward flight. The results were used to classify the importance of key dynamic building blocks on the model fidelity, such as motor/rotor lag dynamics, inertia, and dynamic inflow.

Keywords System identification · Flight mechanics · Electric VTOL (eVTOL)

1 Introduction

Vertical lift multirotor electric aerial vehicles are gaining interest in civilian and military sectors because of their utility in photography, law enforcement, firefighting, package delivery, surveillance and reconnaissance, among many other applications in both the civilian and military sectors. In fact, the FAA predicts that use of commercial (non-model) use of small unmanned aerial systems (which is largely dominated by multirotor electric vehicles) will increase by a factor of 4 by 2022 [1]. Larger vertical lift multirotor electric vehicles (eVTOL) are also being developed because of their potential future role in urban air mobility [2]. The versatility provided by vertical lift, along with the mechanical simplicity of the multirotor configuration, and efficiency of distributed electric propulsion are the key reasons for their popularity. However, these aircraft are unstable when unaugmented and can be difficult to control in winds and turbulence. In addition, one study of drone related air-traffic incidents in our national airspace (during 2013–2015) states that out of 340 incidents, where the drone type was identified in the reports, 246 were multirotor aircraft [3]. To help address the issue of airworthiness, a process for defining unmanned aircraft systems handling qualities has been proposed [4].

Developing standard, well-vetted methods for modeling and simulation, prediction of flying/handling qualities, and control system design is critical for improving safety and quality control of these vehicles. Accurate dynamic modeling is an important element to providing predicted flying/handling qualities, and to developing safe, robust and reliable control systems for all air vehicles, but especially for unstable vehicles, such as multirotor vertical lift aircraft. To address the need for high quality models of multirotor vehicles, this paper demonstrates how system identification models and physics-based models can both provide flight accurate simulation models.

1.1 Background and purpose

Although remotely piloted helicopters have existed since the 1960s [5], modern unmanned vertical lift unmanned

✉ Robert Niemiec
niemir2@rpi.edu

Christina Ivler
ivler@up.edu

Farhan Gandhi
fgandhi@rpi.edu

[1] Center for Mobility with Vertical Lift, Rensselaer Polytechnic Institute, Troy, USA

[2] University of Portland, Portland, USA

[3] San Jose State University Research Foundation, San Jose, USA

Published online: 05 May 2022

aerial systems, which have onboard flight control systems and can navigate autonomously without a remote pilot in the loop, began development in the 1990s. Many of the early unmanned vertical lift systems were conventional helicopter configurations—either converted full-scale manned helicopters (Fire Scout [6], Burro [7]) or miniaturized helicopters (Yamaha R50 [8], Ikarus [9]). As these systems relied on flight control systems for stability, as well as navigation, the development of accurate flight dynamics models and simulators were imperative to the successful design and test of flight control systems and autonomous operations. As such, methods for modeling conventional helicopters were adapted for use in unmanned systems, where now physics-based and system identification modeling methods that had been established for manned helicopters could be directly applied to unmanned systems as described in Refs. [6–9]. The role of system identification began to grow, as the importance of rapid development of unmanned aerial systems was emphasized in Ref. [10]. System identification models and physics-based models can be used hand-in-hand, complimenting each other. System identification provide very accurate linear models at point conditions for accurate flight control design, and can also implemented in a quasi-nonlinear full envelope stitched model [11]. In contrast, physics-based models provide full envelope nonlinear dynamics for flight simulation but often need to be tuned to better match flight data. System identification can only be implemented after the aircraft is constructed and flying, whereas physics-based models can provide dynamics models prior to flight in order to aid design decisions and development of the control system. Once flight test is possible, system identification can be used directly and/or to update the physics-based models [12–14]. For conventional vertical lift aircraft, frequency domain system identification as implemented by the CIFER® software [15], and blade-element physics-based models have been widely used. To address the need for accurate flight dynamics models of electric multirotor vehicles, it is natural to look to methods validated in the past for conventional single-rotor helicopters. In addition, in fact, system identification has been shown to work well for small (52 cm hub-to-hub) electric quadcopters [16, 17], as well as midsize (127 cm hub-to-hub) quadcopter, hexacopters and octacopters [18, 19]. As when applying to any new configuration, methods must be adapted to address the unique challenges and dynamics of the new configuration. Herein, the authors describe how system identification and physics-based blade element models can be used to understand and accurately model the dynamics of multirotor electric unmanned aerial vehicles. For multirotor electric vehicles, this paper provides the following contributions:

Fig. 1 University of Portland hexacopter

Table 1 Specifications for hexacopter

Aircraft	
Weight, with Battery	1550g
Diameter (hub-to-hub)	55cm
Inertia (Swing Test)	
I_{xx}	0.0266 kg m^2
I_{yy}	0.0266 kg m^2
I_{zz}	0.0498 kg m^2
Brushless Motors (6 total)	
Weight, each	47g
K_v	930 RPM/V
Electronic Speed Controller (6 total)	
Current (Continuous)	30A
Weight, each	32g
Rotors (6 total)	
Diameter	25.4cm
Pitch	12cm
Weight, each	10g

- Evaluation of fidelity for both physics-based and system-identification models compared to flight data collected at hover and forward flight
- Documentation of differences in hover versus forward flight dynamics
- Apply system identification results to improve physics-based models of multirotor electric vehicles
- Classify the importance of key dynamic building blocks on the model fidelity of physics-based models, such as motor/rotor lag dynamics, inertia, and dynamic inflow

1.2 Test aircraft

The model used as the example vehicle is the University of Portland hexacopter. It is based on a DJI Flamewheel

F550 frame and has a Pixhawk mini installed onboard. The hexacopter is pictured in Fig. 1, and detailed specifications are listed in Table 1.

2 Modeling methods

Two modeling methods are used to demonstrate flight accurate modeling methods for multirotor aircraft–frequency domain system identification using CIFER® [15] and physics-based modeling methods using Rensselaer Multicopter Analysis Code (RMAC) [20]. The system identification process identifies linear dynamic models of the aircraft from flight test data, so is inherently flight-accurate. System identification and trim data are collected at various flight conditions, and then can be stitched into a full envelope model [12]. The RMAC model is a physics-based model, so is able to simulate nonlinear dynamics of the full envelope and can be easily configured to simulate different multirotor configurations. Linear models can be extracted from the RMAC model. However, the model still must be validated against flight data to ensure flight-accuracy. A more detailed description of each modeling method is given in the following subsections of this paper.

2.1 Frequency-domain system identification

Frequency domain system identification is a process which extracts state-space models of the vehicle from flight data. Several steps are taken to perform system identification of the multirotor vehicle:

1. Frequency sweeps were collected in flight at hover and forward flight (5 m/s). The sweeps are automated and input at the mixer, as shown for the roll sweep in Fig. 2. The data were collected with the autopilot in an attitude command mode ("stabilize-mode" in Ardupilot [21]). Inputs are measured at the input to the mixer, e.g., δ_{lat} for the roll axis sweep, as shown in Fig. 2. The measured outputs include angular rates (p, q, r), angular attitudes (ϕ, θ, ψ), and accelerations (a_x, a_y, a_z).
2. Frequency responses of the multirotor vehicle are identified from the mixer to the aircraft response, for example p/δ_{lat}. Given that the mixer is somewhat nonlinear and not well documented, frequency responses of the mixer are also determined via system identification, from all inputs to all motors (e.g., for roll axis $\delta_{motor,i}/\delta_{lat}$). The mixer is needed for comparison with RMAC which has inputs based on motor RPM, not mixer inputs.
3. A mixing matrix is identified. This is not needed for model identification relative to the mixer inputs (Step 4) but allows conversion from the control axes inputs to the motor inputs, which is needed for later comparison to RMAC. The mixer matrix is identified in the following form:

$$\begin{bmatrix} \delta_{motor,1} \\ \delta_{motor,2} \\ \delta_{motor,3} \\ \delta_{motor,4} \\ \delta_{motor,5} \\ \delta_{motor,6} \end{bmatrix} = \begin{bmatrix} M_{11} & M_{12} & M_{13} & M_{14} \\ M_{21} & M_{22} & M_{23} & M_{24} \\ M_{31} & M_{32} & M_{33} & M_{34} \\ M_{41} & M_{42} & M_{43} & M_{44} \\ M_{51} & M_{52} & M_{53} & M_{54} \\ M_{61} & M_{62} & M_{63} & M_{64} \end{bmatrix} \begin{bmatrix} \delta_{lat} \\ \delta_{lon} \\ \delta_{yaw} \\ \delta_{thr} \end{bmatrix} \quad (1)$$

   where, for example, the M_{11} term would be identified by fitting a gain to the identified frequency response of $\delta_{motor,1}/\delta_{lat}$.
4. Model identification of state-space models relative to the mixer inputs (e.g., δ_{lat} in Fig. 2), is performed by optimizing the parameters in the state-space model to best fit the identified frequency responses from flight data. At hover, decoupled state-space models of the vehicle dynamics are determined for pitch, roll, yaw and heave. The multirotor configuration, which has counter rotating propellers, has negligible coupling of the vehicle dynamics at hover, but some coupling of the pitch/heave response in forward flight. The model structure includes the effect of the motor dynamics, which is modeled as first order lag with time constant ω_{lag}. Due to the decoupled nature of the hexacopter (because of its symmetry and counter rotating rotors) two 3-DOF models are identified. At hover, many of the pitch and roll parameters are constrained between the two decoupled structures at hover to model the symmetry of the dynamics. Equation 2 represents the longitudinal-heave dynamics and Eq. 3 is lateral-directional dynamics:

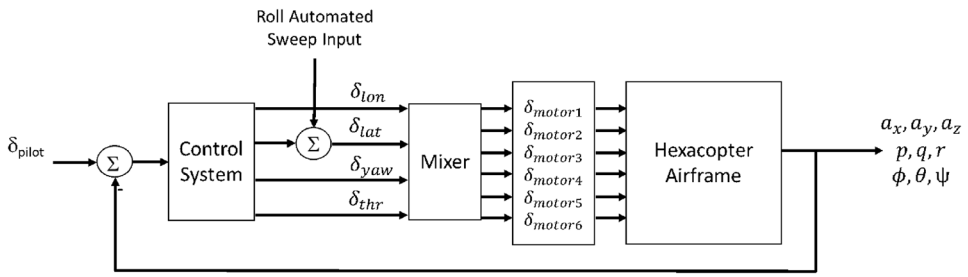

Fig. 2 Block diagram of hexacopter control system and frequency sweep input location

$$\begin{bmatrix} \dot{u} \\ \dot{w} \\ \dot{q} \\ \dot{\theta} \\ \dot{T}_{lon} \\ \dot{T}_{thr} \end{bmatrix} = \begin{bmatrix} X_u & X_w & (-w_0 + X_q) & -g\cos\theta_0 & 0 & 0 \\ Z_u & Z_w & (u_0 + Z_q) & g\sin\theta_0 & Z_{\delta_{lon}} & Z_{\delta_{thr}} \\ M_u & M_w & M_q & 0 & M_{\delta_{lon}} & M_{\delta_{thr}} \\ 0 & 1 & 0 & 0 & 0 & 0 \\ 0 & 0 & 0 & 0 & -\omega_{lag} & 0 \\ 0 & 0 & 0 & 0 & 0 & -\omega_{lag} \end{bmatrix} \begin{bmatrix} u \\ w \\ q \\ \theta \\ T_{lon} \\ T_{thr} \end{bmatrix} + \begin{bmatrix} 0 & 0 \\ 0 & 0 \\ 0 & 0 \\ 0 & 0 \\ \omega_{lag} & 0 \\ 0 & \omega_{lag} \end{bmatrix} \begin{bmatrix} \delta_{lon}(t-\tau) \\ \delta_{thr}(t-\tau) \end{bmatrix} \tag{2}$$

$$\begin{bmatrix} \dot{v} \\ \dot{p} \\ \dot{r} \\ \dot{\phi} \\ \dot{T}_{lat} \\ \dot{T}_{yaw} \end{bmatrix} = \begin{bmatrix} Y_v & w_0 & -u_0 & g\sin\theta_0 & 0 & 0 \\ L_v & L_p & L_r & 0 & L_{\delta_{lat}} & L_{\delta_{yaw}} \\ N_v & N_p & N_r & 0 & N_{\delta_{lat}} & N_{\delta_{yaw}} \\ 0 & 1 & 0 & 0 & 0 & 0 \\ 0 & 0 & 0 & 0 & -\omega_{lag} & 0 \\ 0 & 0 & 0 & 0 & 0 & -\omega_{lag} \end{bmatrix} \begin{bmatrix} v \\ p \\ r \\ \phi \\ T_{lat} \\ T_{yaw} \end{bmatrix} + \begin{bmatrix} 0 & 0 \\ 0 & 0 \\ 0 & N'_{\delta_{yaw}} \\ 0 & 0 \\ \omega_{lag} & 0 \\ 0 & \omega_{lag} \end{bmatrix} + \begin{bmatrix} \delta_{lat}(t-\tau) \\ \delta_{yaw}(t-\tau) \end{bmatrix} \tag{3}$$

The inputs to the model are the longitudinal control input δ_{lon}, lateral control input δ_{lat}, yaw control input δ_{yaw} and the throttle control input δ_{thr}, all measured just upstream of the mixer (in normalized units, %/100). The aircraft velocity states were longitudinal velocity u (ft/s), lateral velocity v (ft/s), vertical velocity w (ft/s). The aircraft angular velocity states were roll rate p (rad/s), pitch rate q (rad/s), and yaw rate r (rad/s). The attitude states were roll attitude ϕ (rad), pitch attitude θ (rad).

Motor lag states T_{lon}, T_{lat}, T_{yaw} and T_{thr} were introduced to each corresponding control input. The associated motor lag ω_{lag} (rad/s) was identified and constrained between all cases for both hover and forward flight. This motor lag represents the physical constraint that the motors cannot provide instantaneous change in thrust (due to the inertia of the motor and rotor blades). This motor lag as well as a lead term ($N'_{\delta_{yaw}}$) affect the yaw rate response over the frequency range of interest. The motor lead frequency that affects the yaw response can be derived from Eq. 3 and takes the form:

$$\omega_{lead} = \omega_{lag}\left(1 + \frac{N_{\delta_{yaw}}}{N'_{\delta_{yaw}}}\right) \tag{4}$$

This model structure and hover system identification of the University of Portland hexacopter is described more fully in Ref. [22].

5. Model Verification is performed against doublets collected in flight to ensure the model also has good predictive capability in the time domain.

3 Rensselaer Multicopter Analysis Code

The Rensselaer Multicopter Analysis Code (RMAC) [20] is a low-cost comprehensive analysis tool designed for use on multirotor vertical lift aircraft, such as the UP hexacopter. The multirotor vehicle is modeled as a 6-DOF, second-order dynamic rigid body. The equations of motion are rewritten in first-order form by introducing kinematic states for the position and attitude of the aircraft, whose derivatives are given by Eqs. 5 and 6, where the 3x3 matrix R represents a rotation matrix which rotates a vector from the body-attached reference frame to the inertial reference frame, and the matrix B expresses the rates of change of the 3-2-1 Euler angles in terms of the body angular velocities:

$$\begin{bmatrix} \dot{x} \\ \dot{y} \\ \dot{z} \end{bmatrix} = R \begin{bmatrix} u \\ v \\ w \end{bmatrix} = R\mathbf{V} \tag{5}$$

$$\begin{bmatrix} \dot{\phi} \\ \dot{\theta} \\ \dot{\psi} \end{bmatrix} = B \begin{bmatrix} p \\ q \\ r \end{bmatrix} = B\boldsymbol{\omega} \tag{6}$$

The linear and angular accelerations of the hexacopter are given by Eqs. 7 and 8, respectively. These equations are obtained through a simple summation of forces and moments about the hexacopter center of gravity. The forces acting on the aircraft include gravity, rotated into the body-attached reference frame, fuselage drag, rotor forces. Fuselage drag and rotor forces induce moments about the center of gravity, with moment arms $\mathbf{r}_d$ and $\mathbf{r}_i$, respectively. In addition, the moments acting about the hub of each rotor, M_i, are also included in Eq. 8. Because these equilibrium equations are resolved in the non-inertial body-attached axes, the Coriolis and inertial coupling effects must be included in Eqs. 7 and 8, respectively:

$$\begin{bmatrix} \dot{u} \\ \dot{v} \\ \dot{w} \end{bmatrix} = R^T \begin{bmatrix} 0 \\ 0 \\ g \end{bmatrix} + \frac{1}{m}\left(\mathbf{D}_{fus} + \sum_{i=1}^{6} \mathbf{F}_i\right) - \boldsymbol{\omega} \times \mathbf{V} \tag{7}$$

$$\begin{bmatrix}\dot{p}\\ \dot{q}\\ \dot{r}\end{bmatrix} = \mathbf{I}^{-1}\left(\mathbf{r}_D \times \mathbf{D}_{fus} + \sum_{i=1}^{6}(\mathbf{M}_i + \mathbf{r}_i \times \mathbf{F}_i)\right) - \boldsymbol{\omega} \times \mathbf{I}\boldsymbol{\omega} \tag{8}$$

where $\mathbf{D}_{fus}$ represents the fuselage drag, parallel to the freestream velocity.

Rotor forces ($\mathbf{F}_i$) and hub moments ($\mathbf{M}_i$) are calculated using blade element theory, and are a function of the speed of the rotor and the linear and rotational velocity of the rotor hub, which are, in turn, functions of the aircraft linear and angular velocity. Rotor induced velocities are modeled using a 10 state, 3x4 Peters-He dynamic wake model, with each rotor possessing its own unique states. The higher frequency states are necessary to capture the steady pitching moment [23]. The dynamics governing the induced flow are given by Eq. 9. The matrices M, V, and L are available in closed form in Ref. [24]. In RMAC, the forcing function τ is phase-averaged over a revolution, so the inflow states α and β are similarly phase-averaged:

$$\begin{aligned}\dot{\alpha} &= \Omega(M^c)^{-1}(\tau^c - V^c(L^c)^{-1}\alpha)\\ \dot{\beta} &= \Omega(M^s)^{-1}(\tau^s - V^s(L^s)^{-1}\beta)\end{aligned} \tag{9}$$

To determine an equilibrium condition, Eqs. 7–9 must be solved such that the accelerations and inflow derivatives are zero. The trim variables available to RMAC are: the pitch and roll attitudes (used to trim longitudinal and lateral accelerations), the inflow states (used to solve the inflow equations), and the six rotor speeds Ω_i (to solve the heave and moment equations). With 10 inflow states per rotor, this results in a system of 66 algebraic equations, to be solved with 68 inputs. To reduce the space of trim solutions to a single unique condition, the multirotor coordinate transform [25], is used to rewrite Ω_i in terms of aircraft-level modes. The transform is given by Eq. 10, where rotor 1 is defined as the front-right rotor, and rotor number increases counter-clockwise as viewed from above:

$$\begin{bmatrix}\Omega_1\\ \Omega_2\\ \Omega_3\\ \Omega_4\\ \Omega_5\\ \Omega_6\end{bmatrix} = \begin{bmatrix}1 & 1/2 & -\sqrt{3}/2 & 1\\ 1 & -1/2 & -\sqrt{3}/2 & -1\\ 1 & -1 & 0 & 1\\ 1 & -1/2 & \sqrt{3}/2 & -1\\ 1 & 1/2 & \sqrt{3}/2 & 1\\ 1 & 1 & 0 & -1\end{bmatrix}\begin{bmatrix}\Omega_0\\ \Omega_{1s}\\ \Omega_{1c}\\ \Omega_{0d}\end{bmatrix} \tag{10}$$

Linear approximations to the dynamics are generated by numerically perturbing the aircraft dynamic states about an equilibrium condition, and using the resulting state derivatives to estimate stability derivatives via centered difference. Similarly, the control inputs are perturbed about an equilibrium condition to determine the control derivatives. This results in a linear, 72 state, 4 input state-space model of Eq. 11. Because the inflow dynamics are very high frequency and stable, the associated states are removed via static condensation, resulting in a 12 state, 4 input state space model (Eq. 12). This is mathematically equivalent to eliminating the derivative terms from Eq. 9 and treating it as an static, algebraic equation instead of an ODE:

$$\begin{bmatrix}\dot{x}_R\\ \dot{x}_I\end{bmatrix} = \begin{bmatrix}A_{RR} & A_{RI}\\ A_{IR} & A_{II}\end{bmatrix}\begin{bmatrix}x_R\\ x_I\end{bmatrix} + \begin{bmatrix}B_R\\ B_I\end{bmatrix}u \tag{11}$$

$$\begin{aligned}\dot{x}_R &= \bar{A}x_R + \bar{B}u\\ \bar{A} &= A_{RR} - A_{RI}A_{II}^{-1}A_{IR}\\ \bar{B} &= B_R - A_{RI}A_{II}^{-1}B_I\end{aligned} \tag{12}$$

4 Models at hover and 5 m/s

This section will describe the linear parametric models of the University of Portland hexacopter that were determined by system identification and RMAC. The model structure shown in Eqs. 2,3 is used in both cases. For the system identification model, theoretical accuracy parameters are provided with the identified stability derivatives. These parameters are critical to the model structure determination process–resulting in removal of stability and control derivatives that have poor theoretical accuracy and as such cannot be identified. Note that in the case of the physics-based RMAC model, theoretical accuracy parameters are not used, because the parameters are extracted directly via perturbation methods from the RMAC model. In some cases, stability or control derivatives that were dropped from the model structure in system identification are present in the RMAC model, because the physics-based model provided a result for that parameter.

4.1 Mixer identification

Frequency sweeps were collected in flight at hover and at 5 m/s. For use in model comparison between RMAC and the identified model, a flight-accurate mixer was needed as described in Sect. 2.1. For each axis, the mixer was identified using the frequency response between the the mixer input and the pulse-width modulated (PWM) command to the motor. This effectively fits a linear model to the nonlinear mixer. There are 24 frequency responses in all–one response from each control axis (δ_{thr}, δ_{lat}, δ_{lon}, δ_{yaw}) to each of the motors ($\delta_{motor,1}$, $\delta_{motor,2}$, $\delta_{motor,3}$, $\delta_{motor,4}$, $\delta_{motor,5}$, $\delta_{motor,6}$). Therefore, each mixer term M_{ij} in Eq. 1 can be identified by fitting the linear range of each of the frequency responses. As an example, the frequency response $\delta_{motor,1}/\delta_{yaw}$ is shown in Fig. 3; the coherence is above 0.6 between 1 and 15 rad/s, a fairly wide frequency range. Because we are fitting a static

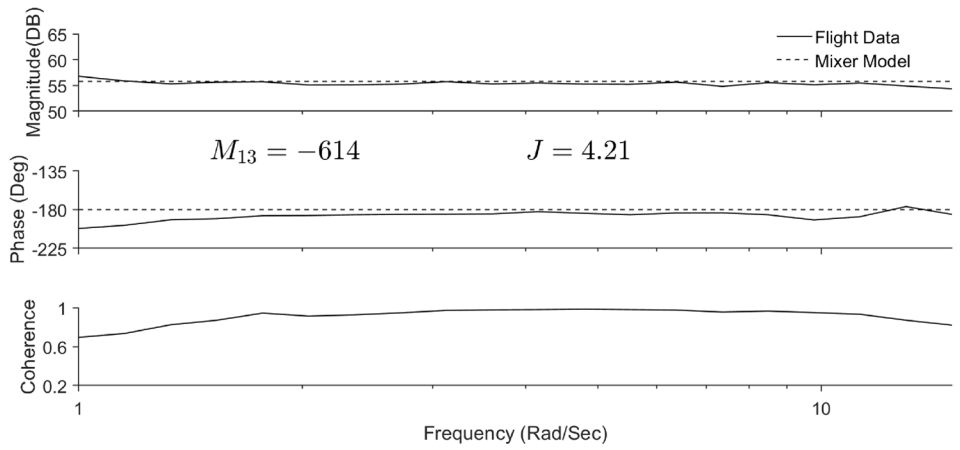

Fig. 3 Identified mixer frequency response for $\delta_{motor,1}/\delta_{yaw}$

gain to this frequency response, the magnitude of M_{ij} is chosen to best fit the magnitude response, and the sign is either ± 1, depending on the identified phase (0° corresponds to positive sign, and $\pm 180°$ corresponds to a negative sign). The static gain fits the frequency response excellently, with a cost $J = 4.21$. Considering all of the elements of the mixer, the average cost $J_{ave} = 30.72$, indicating a very good model (according to guidelines established in Ref. [15]).

4.2 System identification models

The flight records were then processed using the CIFER® software to determine non-parametric frequency responses models from these data. Note that due to the largely decoupled nature of the hexacopter at hover, the responses were considered as single input. No multi-input processing to remove the effects of off-axis inputs was performed at hover. For forward flight, some aerodynamic and kinematic coupling is present, and as such multi-input analysis and processing was performed. The identification process directly provides the linearized stability derivatives and their theoretical accuracy parameters. The resulting hover and forward flight models are shown in Table 2. Note that any parameters not shown in the table have values of zero for both flight conditions. Cramer Rao (CR) and Insensitivity (I) are theoretical accuracy parameters. It is desired that $CR < 20\%$ and $I < 10\%$, which indicates the parameter is sensitive and uncorrelated to any other parameters. When a parameter has borderline theoretical accuracy, it is retained in the model structure, because the model fit requires that term for a good prediction of flight data. This was the case of the L_p and M_q parameters in forward flight. However, at hover these parameters were very insensitive and as such were dropped from the model structure and set to zero without compromising model fit.

It should be noted that in several cases, the model was constrained to ensure that symmetry in the physics was retained. For example, at hover the model structure was setup so that $X_u = Y_v$ and that $L_v = -M_u$. In addition, the motor lag dynamics were fixed at 15 rad/s, which was determined based on the dynamics at hover and then fixed in the forward flight identification. As one may observe in Eq. 3, the motor lag dynamics were supplemented with a lead input $N'_{\delta_{yaw}}$. The yaw input is generated by differential torque on the motors, not the motor thrust as in the other control inputs, and has been observed to have a lead-lag characteristic [18]. For this aircraft, the lead zero is at $\omega_{lead} = 5.1$ rad/s as calculated by Eq. 4 and the lag pole at $\omega_{lag} = 15$ rad/s. From Table 2, the following conclusions about the hexacopter dynamics in hover versus forward flight can be drawn:

1. Speed damping derivatives L_v and M_u, which largely dominate the roll and pitch dynamics at hover, are somewhat reduced in forward flight.
2. Pitch and roll damping (L_p and M_q) play a larger role in the dynamics of forward flight; however, the theoretical accuracy is borderline, considering that ideally $I < 10\%$ and $CR < 20\%$. The authors observed that the models did not fit the flight data as well in forward flight with these parameters set to zero, so the parameters were retained in the model structure despite slightly degraded theoretical accuracy.
3. Coupling between pitch and heave becomes more prevalent in forward flight, where M_w and $M_{\delta_{thr}}$ derivatives are identified with non-zero values. This is similar in behavior to a helicopter at forward flight.
4. Motor lag, lead and time delay are constant across both flight conditions.

Table 2 SystemID stability and control derivatives

Linear model elements	Stability derivatives					
	Hover			5 m/s		
	Value	CR (%)	I (%)	Value	CR (%)	I (%)
X_u (1/s)	− 0.221	–	–	− 0.202	11.06	2.61
Y_v (1/s)	− 0.221	–	–	− 0.287	12.41	5.69
Z_w (1/s)	− 0.338	21.1	10.3	− 0.537	8.28	3.12
L_v (rad/(m·s))	− 4.01	5.21	1.88	− 3.18	10.4	2.96
L_p (1/s)	0	–	–	− 0.895	30.96	13.0
M_u (rad/(m·s))	4.01	5.21	1.88	2.05	22.12	1.97
M_q (1/s)	0	–	–	− 0.357	41.4	21.09
M_w (rad/(m·s))	0	–	–	− 0.305	17.64	0.981
N_r (1/s)	0	–	–	− 0.510	4.04	1.97
ω_{lag} (1/s)	15	5.16	2.07	15	–	–
u_0 (m/s)	0	–	–	5	–	–
w_0 (m/s)	0	–	–	− 0.5	–	–
θ_0 (deg)	0	–	–	− 6	–	–
	Control derivatives					
	Value	CR (%)	I (%)	Value	CR (%)	I (%)
$Z_{\delta_{thr}}\left(\frac{m/s^2}{\%/100}\right)$	− 39.4	2.29	1.35	− 39.5	2.9	1.03
$L_{\delta_{lat}}\left(\frac{rad/s^2}{\%/100}\right)$	145	2.93	2.11	141	2.72	1.23
$M_{\delta_{lon}}\left(\frac{rad/s^2}{\%/100}\right)$	165	3.78	1.21	156	2.06	0.981
$M_{\delta_{thr}}\left(\frac{rad/s^2}{\%/100}\right)$	0	–	–	− 5.51	8.70	2.15
$N_{\delta_{lat}}\left(\frac{rad/s^2}{\%/100}\right)$	0	–	–	− 3.62	4.81	2.4
$N'_{\delta_{yaw}}\left(\frac{rad/s^2}{\%/100}\right)$	31.2	9.68	1.51	30.3	4.04	1.97
$N_{\delta_{yaw}}\left(\frac{rad/s^2}{\%/100}\right)$	− 22.9	6.03	0.914	− 19.2	-	-
τ (s)	0.02	9.43	4.71	0.02	-	-

5 RMAC models

Stability derivatives were estimated by perturbing each of the dynamic states (including inflow states) from an equilibrium value, and numerically estimating the derivative using a centered difference formula. The estimated values of the stability derivatives are tabulated in Table 3. There are no motor dynamics included explicitly in the RMAC model, these are added as simple first-order filtering functions based on the system identification results. Parameters not shown below are near zero. The time delay as identified in system identification is also included as a filter on the input.

6 Validation against flight data

The fidelity of both the system identification and linearized RMAC models were carefully evaluated against flight data in the frequency and time domains. Validation was performed at hover and forward flight. The results for both system ID and RMAC were overlaid to provide insight to the predictive accuracy of each model, and highlight their relative abilities to simulate the measured flight dynamics.

Table 3 RMAC-predicted stability and control derivatives

Stability derivatives			Control derivatives		
Linear model element	Hover	5 m/s	Linear model element	Hover	5 m/s
X_u (1/s)	− 0.061	− 0.35	$Z_{\delta_{lon}}\left(\frac{m/s^2}{\%/100}\right)$	0	0
Y_v (1/s)	− 0.061	− 0.20	$Z_{\delta_{thr}}\left(\frac{m/s^2}{\%/100}\right)$	− 47.1	− 45.7
Y_p (m/(rad·s))	0	− 0.5	$L_{\delta_{lat}}\left(\frac{m/s^2}{\%/100}\right)$	146	141
Z_w (1/s)	− 0.93	− 1.28	$L_{\delta_{yaw}}\left(\frac{m/s^2}{\%/100}\right)$	0	− 4.66
L_v (rad/(m·s))	− 1.62	− 1.29	$M_{\delta_{lon}}\left(\frac{m/s^2}{\%/100}\right)$	137	133
L_r (1/s)	0	0.76	$M_{\delta_{thr}}\left(\frac{m/s^2}{\%/100}\right)$	0	4.34
M_u (rad/(m·s))	1.62	0.83	$N_{\delta_{lat}}\left(\frac{m/s^2}{\%/100}\right)$	0	− 0.99
N_r (1/s)	− 0.16	− 0.14	τ (s)	0.02	0.02
ω_{lag} (rad/s)	15	15	ω_{lead} (rad/s)	5.1	5.1

6.1 Frequency domain cost functions

Frequency domain validation of the models is performed qualitatively with visual overlay of the models against flight data, and quantitatively with a cost function. The cost function is calculated by a weighted sum of time and frequency domain errors [15]:

$$J_i = \frac{20}{n_\omega}\sum_{\omega_1}^{\omega_{n_\omega}} W_\gamma\Big[W_g(|\hat{T}_c(\omega)| - |T(\omega)|)^2 + W_p\big(\angle\hat{T}_c(\omega) - \angle T(\omega)\big)^2\Big] \tag{13}$$

where $|T|$ and $\angle T$ are flight frequency response magnitude (dB) and phase (deg), $|\hat{T}_c|$ and $\angle\hat{T}_c$ are the model frequency response magnitude (dB) and phase (deg). Magnitude and phase error weightings are $W_g = 1$ and $W_p = 0.01745$. The coherence (γ) weighting factors the most accurate (highest coherence) data more heavily in the cost function, where $W_\gamma = 2.5(1 - e^\gamma)^2$.

An individual cost function J_i is calculated for each of i frequency responses that are included in the parametric model identification. A cost $J_i < 50$ indicates a very accurate model for that response, and a cost of $J_i < 100$ is considered an acceptable level of fidelity. The average cost over all frequency responses is used as a metric of overall model fidelity, where $J_{ave} < 100$ is recommended:

$$J_{ave} = \frac{1}{n_{TF}}\sum_{i=1}^{n_{TF}} J_i \tag{14}$$

The cost functions are evaluated for both system ID and RMAC models, as shown in Table 4. The table shows that system ID models are in the excellent range for the most part, as expected considering they are extracted from flight data. Although the RMAC costs are significantly higher for the full frequency range, Table 4 shows that the RMAC models are near the range of $J_{ave} \approx 100$ if the low frequency ($\omega < 5$ rad/s) portion of the response is not used in the cost function calculation ($\omega_{min} = 5$). This indicates that the physics-based models are accurate in the frequency range, where the aircraft responds, such as a first order system and the low frequency unstable oscillatory modes are attenuated.

The frequency response validation plots in Figs. 4, 5, 6, 7, 8, 9, 10 and 11 show the flight data, system identification models and RMAC models. These results clearly illustrate that the system identification models have an excellent fit, and that RMAC predicts the behavior well for most responses at $\omega > 5$ rad/s for both hover and forward flight. This can also be seen in the eigenvalues shown in Table 5 for hover and Table 6 for forward flight. At these higher frequencies, the unstable oscillatory modes has attenuated and the 1st order modes as well as control power dominate the response, which RMAC predicts with good accuracy.

Although the RMAC model does not well predict low frequency behavior, it does provide an acceptable fit in the frequency range that is most important for flight control. For control system design, the model should be accurate over the range of $\frac{1}{3}\omega_c < \omega < 3\omega_c$. To determine the expected crossover frequency of the hexacopter, Froude scaling relative to a representative full scale aircraft, the UH-60, is used. For the UH-60, a reasonable crossover is 3 rad/s, and the scale factor is $N = \frac{D_{hub-to-hub}}{D_{UH-60}} = 29.8$, so that the hexacopter scale crossover frequency is $\omega_c = 3\sqrt{N} = 16.4$ rad/s. This indicates that the RMAC model (which has acceptable accuracy in the range of $5 < \omega < 50$ rad/s) would be sufficient for

Table 4 Frequency domain model validation costs (J) for hover and forward flight

Frequency Response	Hover			
	Frequency Range (rad/s) $\omega_{min} - \omega_{max}$	Cost, J		
		System ID	RMAC	RMAC with $\omega_{min} = 5$
a_x/δ_{lon}	0.6–22	50.4	190	143
$\dot{u}/\delta_{lon}$	0.6–30	86.2	535	196
q/δ_{lon}	0.6–50	58.9	422	136
a_y/δ_{lat}	0.3–25	59.7	177	108
$\dot{v}/\delta_{lat}$	0.5–30	79.9	689	91.5
p/δ_{lat}	0.3–50	52.0	524	90.8
r/δ_{yaw}	1.5–20	25.1	34.8	30.8
$\dot{w}/\delta_{thr}$	0.6–25	13.1	68	82.4
J_{ave}		52.2	330	110
	5 m/s			
	Frequency Range (rad/s) $\omega_{min} - \omega_{max}$	Cost, J		
		System ID	RMAC	RMAC with $\omega_{min} = 5$
a_x/δ_{lon}	9–35	96.4	270	270
$\dot{u}/\delta_{lon}$	5–30	49.1	203	203
q/δ_{lon}	4–50	63.0	148	139
$\dot{w}/\delta_{lon}$	5–30	52.9	232	232
a_y/δ_{lat}	0.8–25	49.6	227	102
$\dot{v}/\delta_{lat}$	1.1–20	43.9	204	104
p/δ_{lat}	4–35	34.7	135	123
r/δ_{yaw}	1–12	25.8	109	56.4
a_z/δ_{thr}	0.7–22	17.4	94.4	66.3
$\dot{w}/\delta_{thr}$	0.4–12	47.0	551	82.1
J_{ave}		48.0	217	127

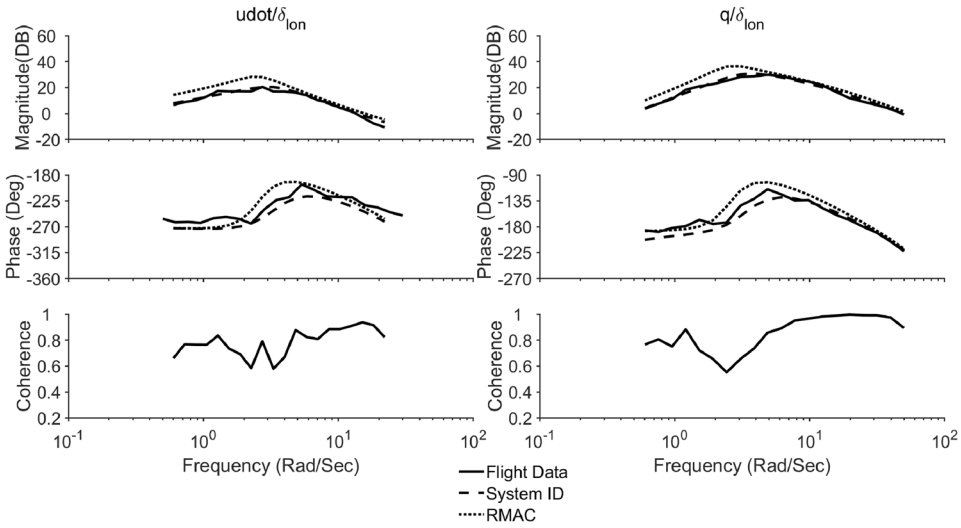

Fig. 4 Hover validation for longitudinal velocity rate (m/s^2) and pitch rate (rad/s) to longitudinal input (%/100)

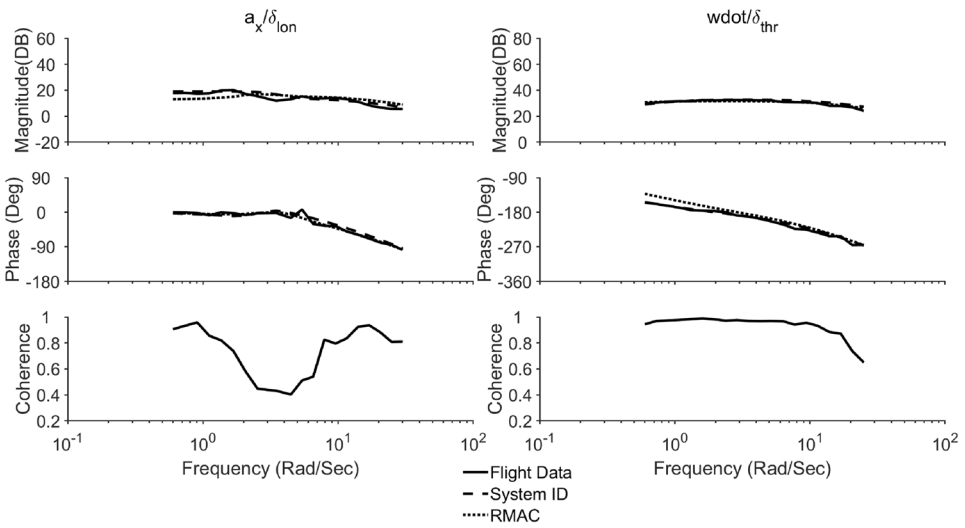

Fig. 5 Hover validation for longitudinal acceleration (m/s^2) to longitudinal input (%/100) and vertical velocity rate (m/s^2) to throttle input (%/100)

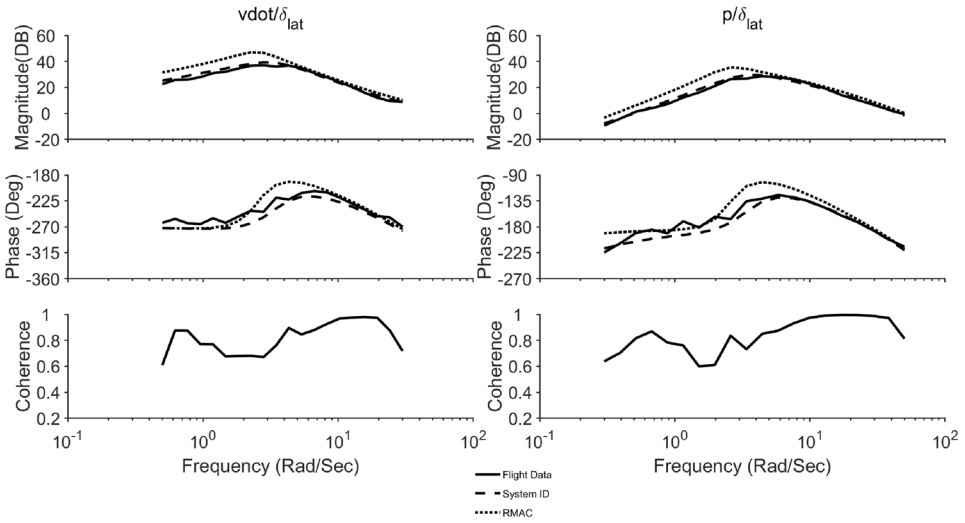

Fig. 6 Hover validation for lateral velocity rate (m/s^2) and roll rate (rad/s) to lateral input (%/100)

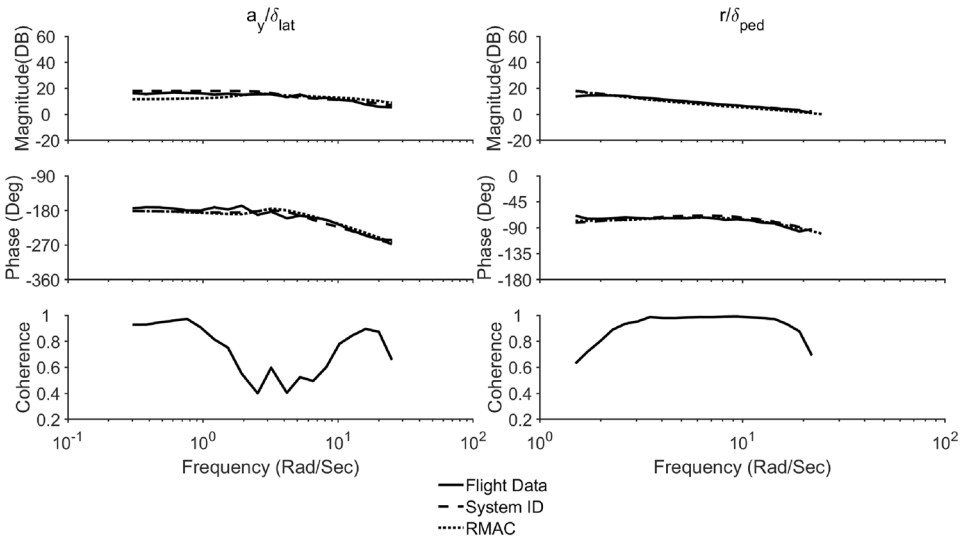

Fig. 7 Hover validation for lateral acceleration (m/s^2) to lateral input (%/100) and yaw rate (m/s^2) to pedal input (%/100)

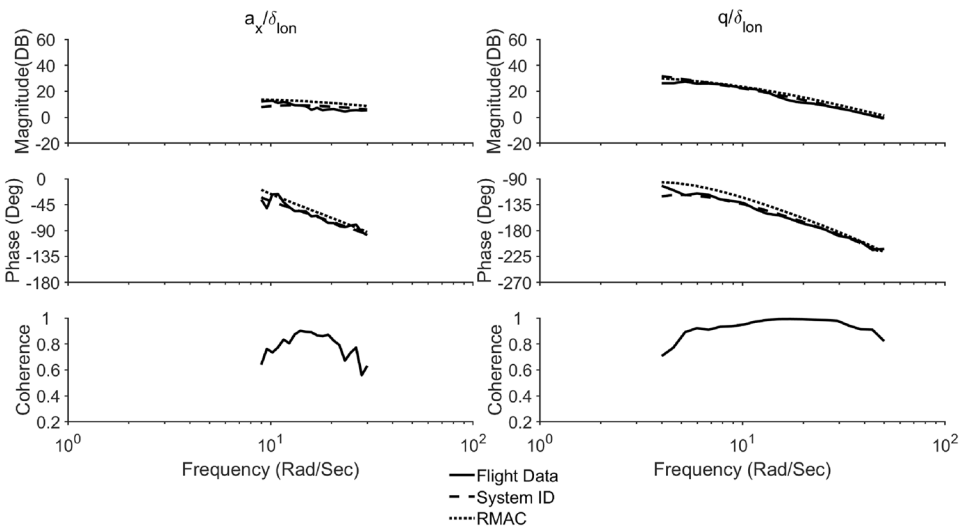

Fig. 8 Validation at 5m/s for longitudinal acceleration (m/s^2) and pitch rate (rad/s) to longitudinal input (%/100)

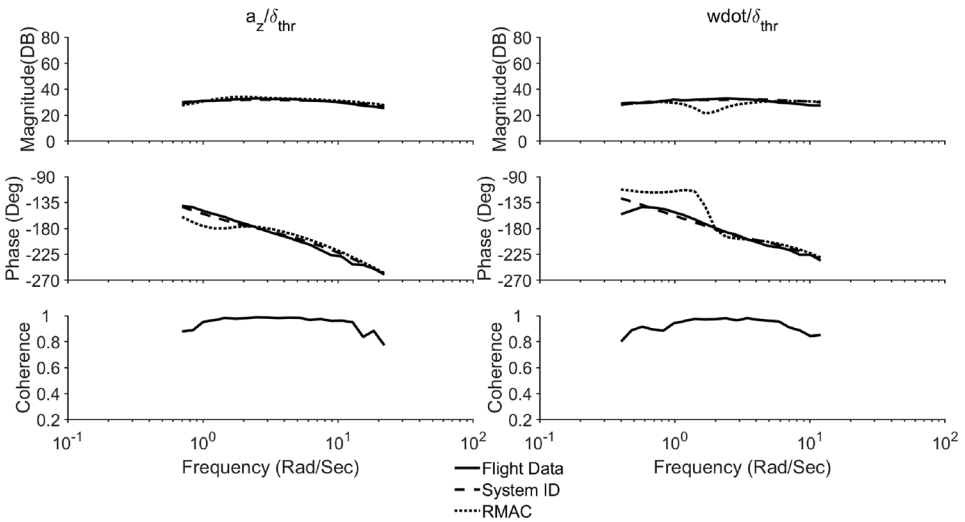

Fig. 9 Validation at 5 m/s for vertical acceleration (m/s^2) and vertical velocity rate (m/s^2) to throttle input (%/100)

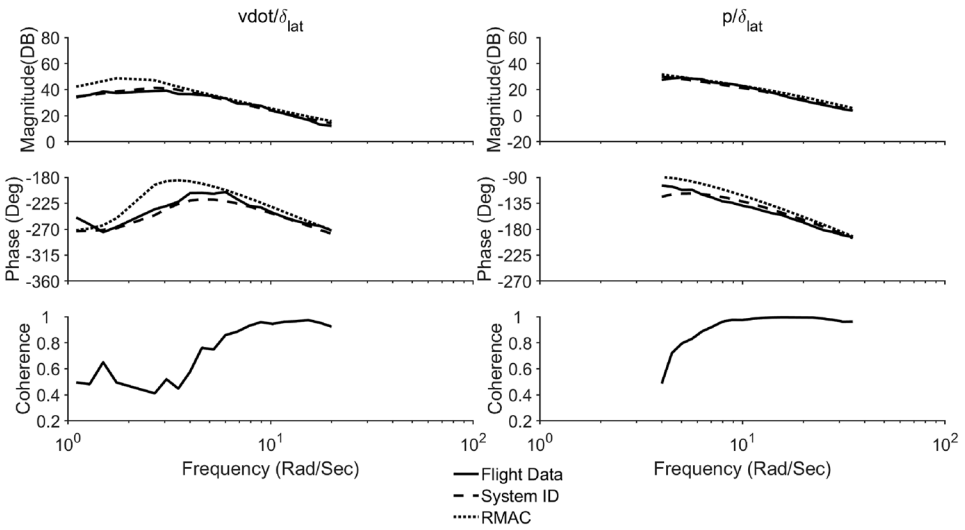

Fig. 10 Validation at 5 m/s for lateral velocity rate (m/s^2) and roll rate (rad/s) to lateral input (%/100)

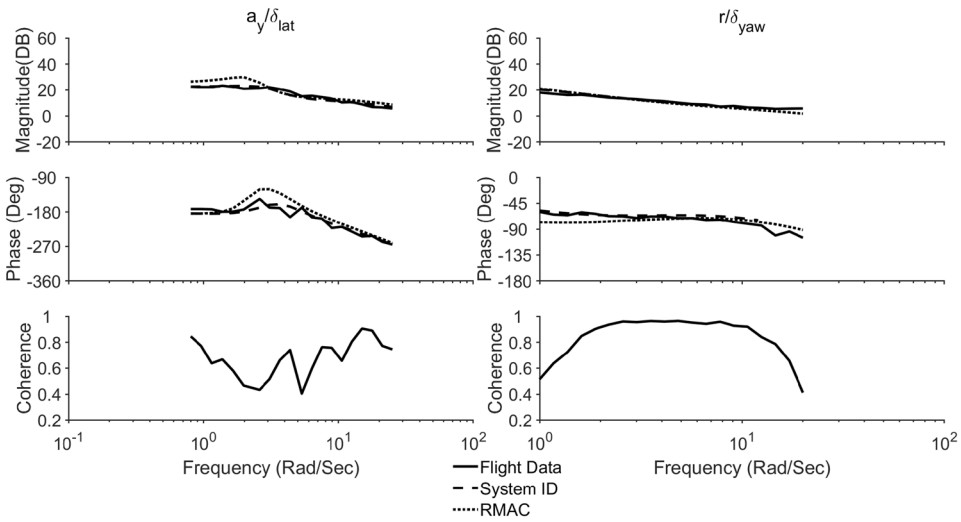

Fig. 11 Validation at 5 m/s for lateral acceleration (m/s^2) to lateral input (%/100) and yaw rate (m/s^2) to pedal input (%/100)

Table 5 Eigenvalues at hover for system ID model and RMAC model

	System ID		RMAC	
	Frequency (rad/s)	Damping Ratio	Frequency (rad/s)	Damping Ratio
Roll mode (1st Order)	3.49	1	3.71	1
Pitch mode (1st Order)	3.49	1	3.71	1
Yaw mode (1st Order)	0	1	0.138	1
Pitch oscillating mode	3.35	− 0.48	2.55	− 0.34
Roll oscillating mode	3.35	− 0.48	2.55	− 0.34
Heave mode (1st Order)	0.338	1	0.731	1

Table 6 Eigenvalues at 5 m/s for system ID model and RMAC model

	System ID		RMAC	
	Frequency (rad/s)	Damping Ratio	Frequency (rad/s)	Damping Ratio
Roll mode (1st order)	3.75	1	5.26	1
Pitch mode (1st order)	2.72	1	4.01	1
Yaw mode (1st order)	0.51	1	0.13	1
Pitch oscillating mode	2.55	-0.425	1.27	-0.545
Roll oscillating mode	2.88	-0.445	2.02	-0.281
Heave mode (1st Order)	0.587	1	0.589	1

control system design, although building in additional stability margin would be prudent given the elevated model cost. Clearly, a system identification model will provide less uncertainty in the control system design, and allow for a more optimal performing control system with less overdesign. However, in the case, where system identification models are not available or practical, such as for first-flight control system gain tuning, evaluation of notional designs prior to construction, or for preliminary design studies–these results indicate that a physics-based model such as RMAC can provide an acceptable prediction of the behavior.

7 Time domain validation

Time domain verification of system identification models is an important last step to validating a system identified model that was developed in the frequency domain [15]. In time domain verification it is critical to test the robustness of the model against a different data set using a different input, to ensure that the system ID model is not overly tuned to the data used to generate the frequency responses from which the model was fit. Robustness to input type is a key indicator that the models represent the physics, as opposed to being a generic curve fit of the data. For RMAC, time domain verification provides important insights on the predictive capability of the model that are difficult to visualize in the frequency domain. The time domain verification costs are shown in Table 7, using the equation:

$$J_{rms} = \sqrt{\frac{1}{n_t n_o} \sum_{i=1}^{n_t} (y_{data} - y)^T W (y_{data} - y)} \tag{15}$$

The desired time domain cost for full-scale vehicles has been well-vetted in Ref. [15], which states that excellent predictive accuracy is $J_{rms} = 1$, although $1 < J_{rms} < 2$ is still considered acceptable. For this smaller vehicle, Froude scaling relative to the UH-60 ($N = \frac{D_{hub-to-hub}}{D_{UH-60}} = 29.8$) was implemented to scale the costs. After scaling, it was determined that $J_{rms} < 5.5$ corresponds to an excellent prediction, but a range from $5.5 < J_{rms} < 11$ was acceptable.

A normalized cost function, the Theil Inequality Coefficient (TIC) does not need to be scaled, and is given by

Table 7 Time domain verification costs for system ID and RMAC models at hover and 5 m/s

	System ID				RMAC			
	Hover		5 m/s		Hover		5 m/s	
	J_{rms}	*TIC*	J_{rms}	*TIC*	J_{rms}	*TIC*	J_{rms}	*TIC*
LAT	1.9	5.3%	2.20	6.9%	2.5	6.6%	3.52	10%
LON	1.5	4.1%	3.12	9.3%	2.8	7.2%	4.29	12%
YAW	0.95	5.2%	2.6	15.8%	1.12	6.4%	3.4	21%
THRUST	0.53	23%	1.67	35%	0.56	24%	8.93	71%

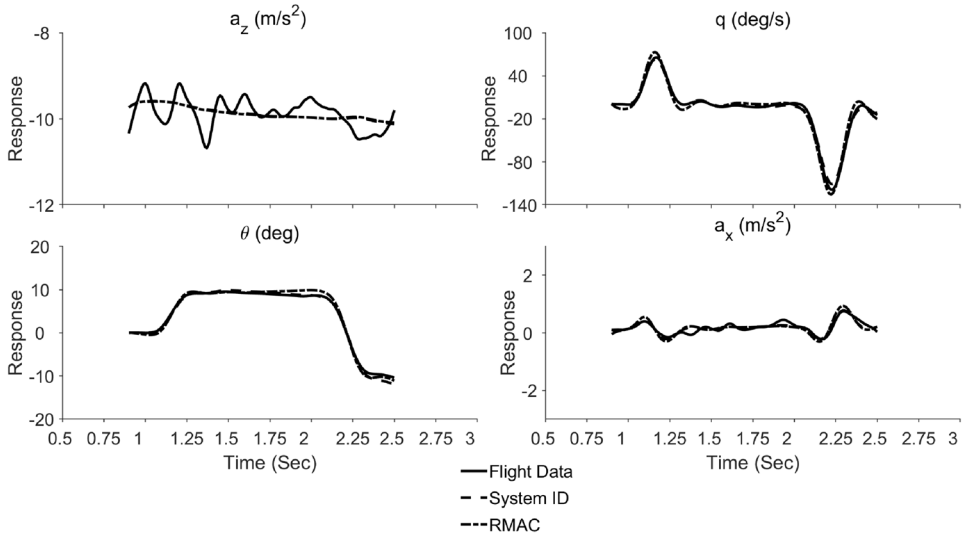

Fig. 12 Hover pitch input time domain verification

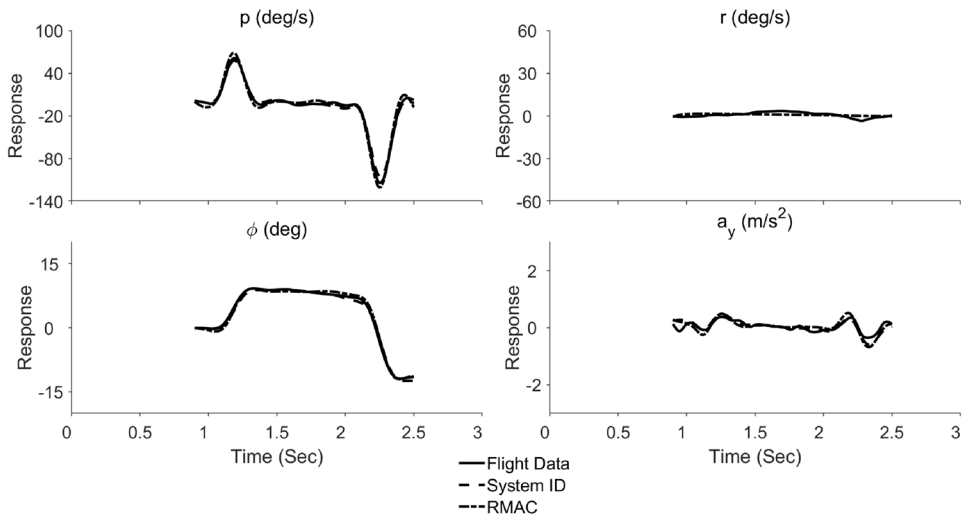

Fig. 13 Hover roll input time domain verification

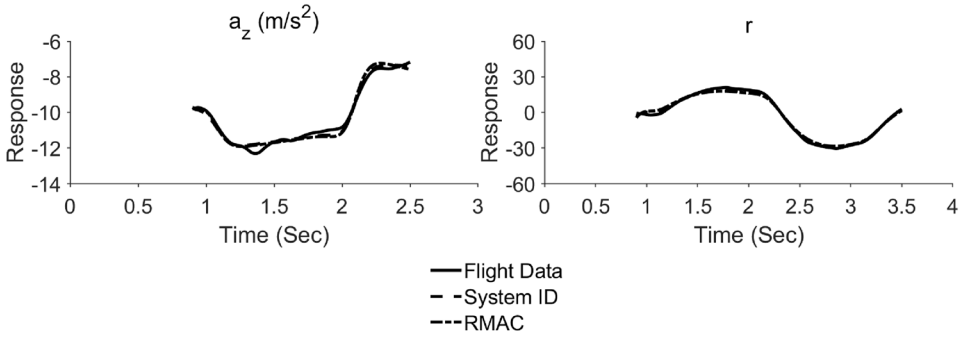

Fig. 14 Hover heave input (left) and yaw input (right) time domain verification

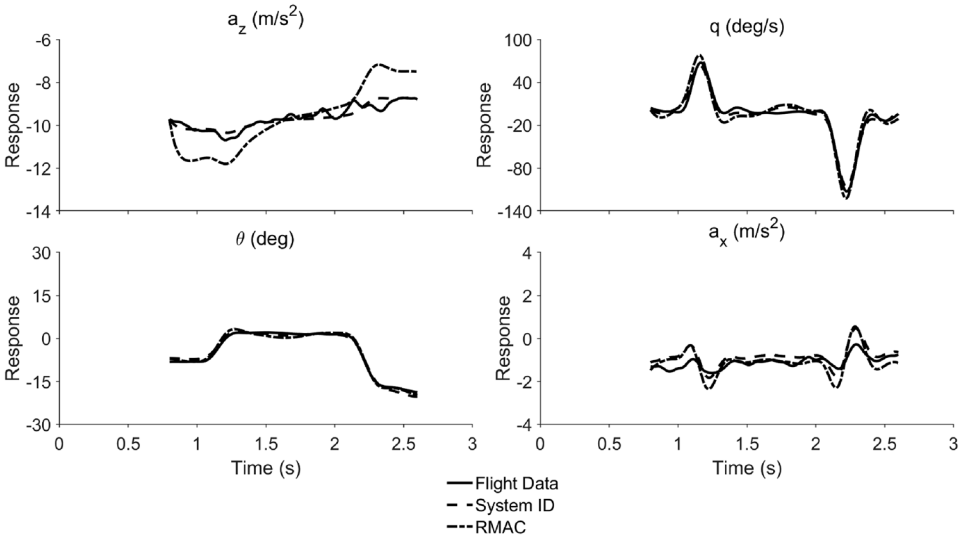

Fig. 15 Forward flight (5 m/s) pitch input time domain verification

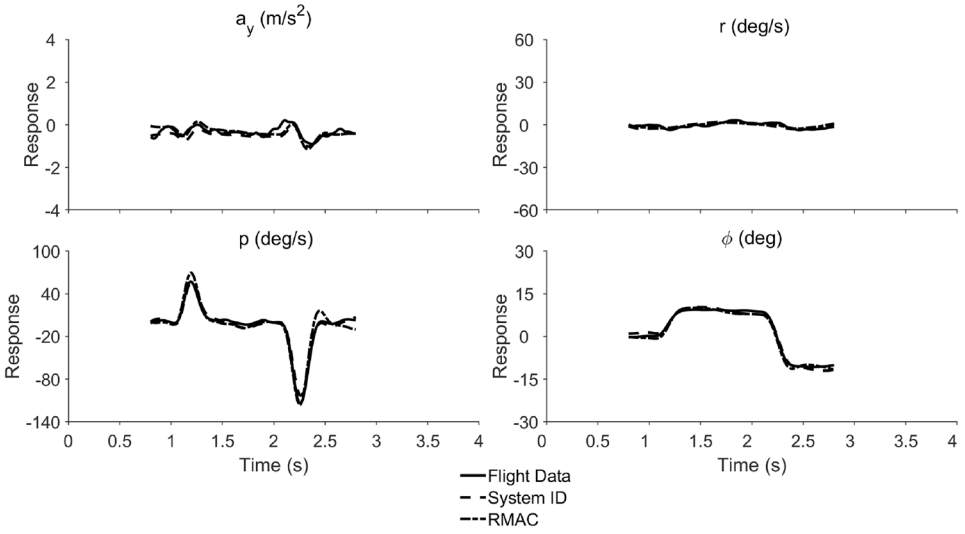

Fig. 16 Forward flight (5 m/s) roll input time domain verification

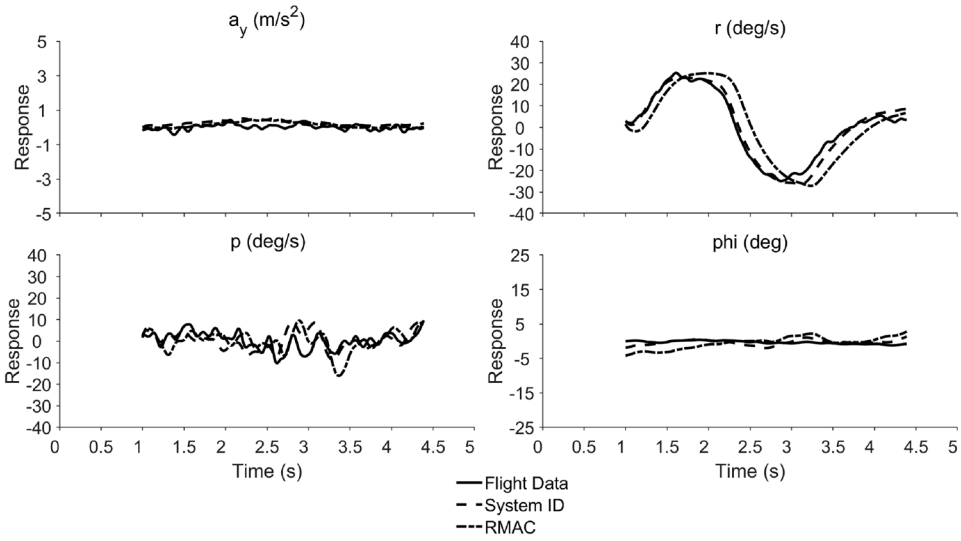

Fig. 17 Forward flight (5 m/s) yaw input time domain verification

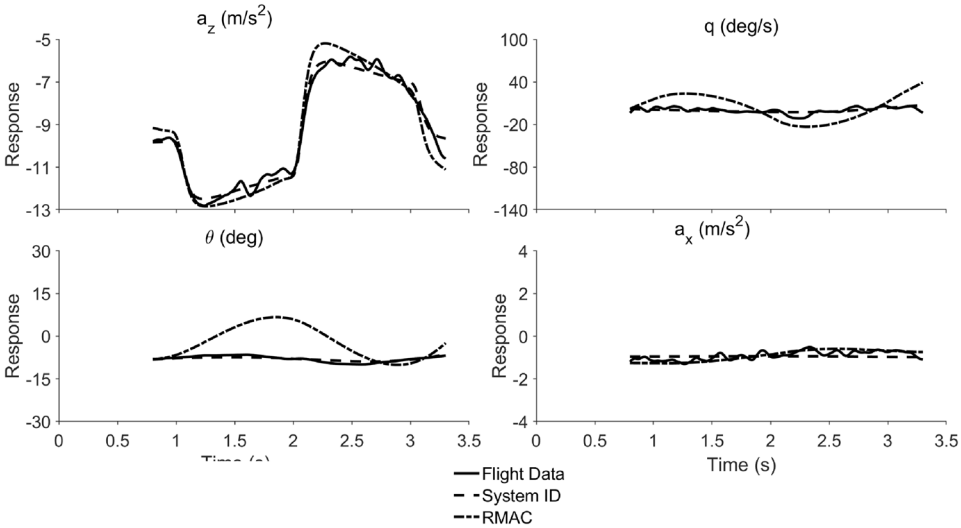

Fig. 18 Forward flight (5 m/s) heave input time domain verification

$$TIC = \frac{J_{rms}}{\sqrt{\frac{1}{n_t n_o}\sum_{i=1}^{n_t} y^T W y} + \sqrt{\frac{1}{n_t n_o}\sum_{i=1}^{n_t} y_{data}^T W y_{data}}} \tag{16}$$

This cost function can be considered as a percent error when multiplied by 100. For good predictive accuracy, it is recommended in Ref. [15] that $TIC < 35\%$.

The time domain cost functions for the system ID and RMAC models are shown in Table 7. The results indicate that the system ID model has excellent predictive accuracy, because its J_{rms} and TIC costs are well below the guidelines for both hover and forward flight. The excellent prediction of the system identification model can be seen in Figs. 12, 13 and 14 for hover, and in Figs. 15, 16, 17 and 18 for the 5 m/s forward flight case. In most of these plots, the system ID model is nearly indistinguishable from the flight data. The RMAC models have J_{rms} and TIC costs that are within the guidelines, indicating good predictive accuracy, for both hover and forward flight, in all responses except for the forward flight thrust response. As shown in Figs. 12, 13 and 14, for hover, the prediction of the RMAC model is also quite good with some magnitude overshoot and phase differences relative to flight data, as also shown in the frequency domain. For forward flight, in Figs. 15 and 16 , the pitch and roll RMAC responses have good predictive accuracy, with slightly larger overshoot relative the flight data than seen in hover. The vertical velocity response during the pitch doublet in Fig. 15 is somewhat over predicted but the response is small and as such the costs are still within the recommended range. The RMAC yaw response has the right shape and magnitude of response, as shown in Fig. 17, but has some phasing mismatch, as also seen in the frequency domain. The yaw-to-roll coupling appears to be well predicted by RMAC in forward flight. The thrust response has reasonable

on-axis prediction of $\dot{w}$ and a_z (although with some overshoot), as shown in Fig. 18, but the off-axis coupling of the pitch rate q and attitude θ is significantly over-predicted.

8 Discussion of dynamics for multirotor vehicles

The time and frequency domain results overall indicate that the RMAC provides acceptable accuracy for preliminary control system design–indicating that a blade element model with a 10 state Peters-He inflow, combined with system identified motor dynamics has reasonably good predictive accuracy in the frequency range of interest at hover and forward flight. Although there are areas for improvement, many of the areas, where dynamic response mismatch occurs would be suppressed by a control system–such as low frequency responses and off-axis coupling. If relying on this model for control system design, it would be wise to design additional robustness into the control system by way of extra gain and phase margin to account for these discrepancies. Still, the match is reasonably good and in the range of acceptable but not excellent fit–this is really as good as you are likely to get with a physics-based model that has not been tuned with empirical corrections to better match flight data. System identification models can play a key role in updating physics-based models and provide guidance for model improvement. Key lessons learned by comparison of these two methods for modeling the dynamics of multirotor vehicles are presented in the following sub-sections of this paper. Several elements were found to be critical in achieving good model fidelity relative to the flight data:

1. Speed and rate damping derivatives
2. Longitudinal and heave coupling
3. Mass moment of inertia
4. Motor dynamics
5. Fuselage lrag
6. Rotor modeling

8.1 Speed and rate damping derivatives

The RMAC blade element model over-predicts the magnitude and phase of the on-axis p/δ_{lat} and q/δ_{lon} responses for frequencies below 5 rad/s, largely stemming from mismatch of the oscillatory mode frequencies as shown by the eigenvalues (Table 5) and seen in the frequency responses of Figs. 4 and 6 . The root cause of the frequency mismatch is related to over-prediction of angular rate damping (L_p and M_q), with simultaneous under-prediction of the speed damping (L_v and M_u). By directly modifying the linear RMAC model, a significant improvement can be seen by reducing rate damping by a factor of two while simultaneously increasing the speed damping by a factor of two, as shown in Fig. 19. These derivatives are all influenced by variations of inflow over the rotor disk as well as differences in inflow between rotors which create relative pitch/roll moments. As such, the discrepancy could possibly be due to interference effects, which are not included in the RMAC model, but the root cause is still an area of investigation.

8.2 Longitudinal/heave coupling

A key area for future improvement of the RMAC model is related to the pitch to heave coupling in forward flight. The mismatch is very clear from the time verification, as shown in Fig. 18. This overprediction of coupling also creates a mismatch at frequencies < 5 rad/s in the $\dot{w}/\delta_{thr}$ frequency domain

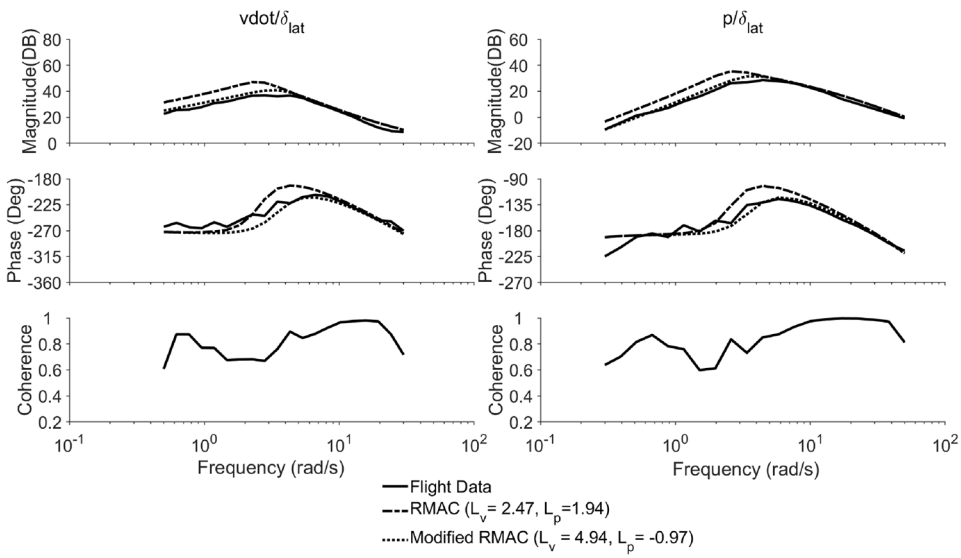

Fig. 19 Direct adjustments fo linearized hover RMAC model to better capture flight response

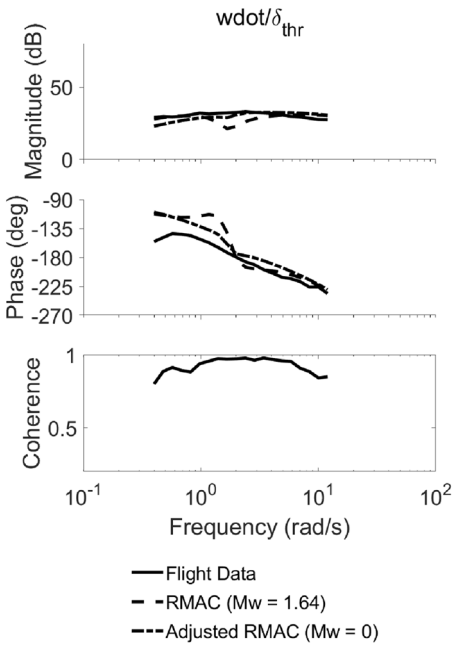

Fig. 20 Adjusted pitch/heave coupling in 5 m/s linearized RMAC model

response, as shown in Fig. 9. The low frequency $\dot{w}/\delta_{thr}$ is largely dominated by the kinematic coupling with the pitch response via the u_0/q term, and so is affected by the pitch/heave coupling. By eliminating the M_w term from the linear RMAC model, both the frequency and time domain responses better predict the flight behavior, as shown in Figs. 20 and 21. The reason for this mismatch is likely a related phenomenon to the mismatch of the speed damping derivative M_u, discussed in the previous section. It should be noted that the coupling control derivative $M_{\delta_{thr}}$ is retained unaltered in this analysis.

8.3 Mass moment of inertia

A key element in accurate representation of any dynamics system, and a well-known source of uncertainty, is the mass moment of inertia. For system identification, the moment of inertia is identified as part of the lumped stability or control derivative. For example, the M_u term is identified as a lumped term that includes the inertia and the aerodynamic effect in pitching moment due to longitudinal velocity:

$$M_u = \frac{1}{I_{yy}} \frac{dM}{du} \tag{17}$$

As such, the inertia is fully correlated with the aerodynamic term and cannot be extracted via system identification.

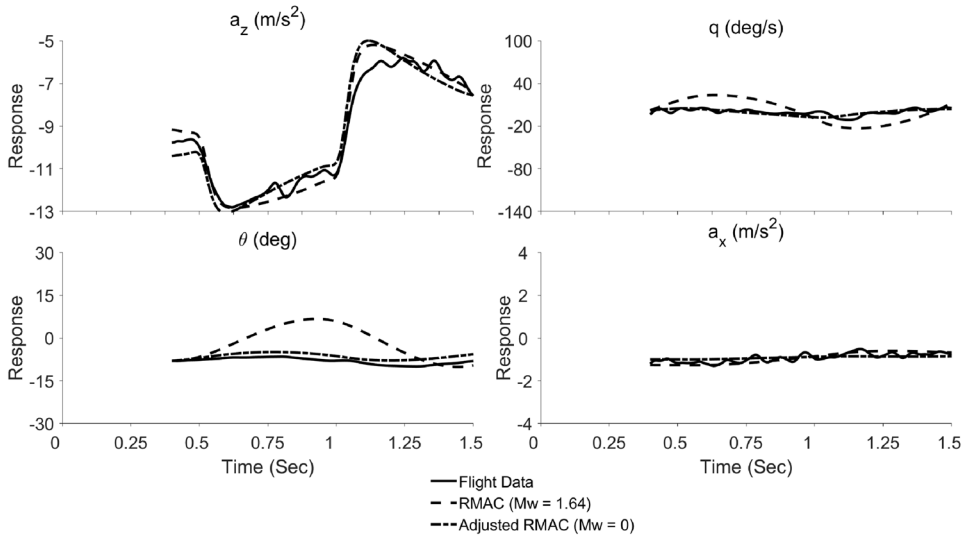

Fig. 21 Direct adjustments to pitch/heave coupling in the forward flight linearized RMAC model

Table 8 Mass moment of inertia for the university of Portland hexacopter

Element	Modeled as	Mass	I_{xx}	I_{yy}	I_{zz}
Center plate with sensors, and pixhawk	Thin disk with diameter of 16.5cm	830g	0.00565	0.00565	0.0113
Arms (6)	Point Masses at 17.8cm from center	342g	0.0054	0.0054	0.0108
Motors/Blades (6)	Point masses at 27.5cm from center	384g	0.0143	0.0143	0.0285
Total	Sum of elements	1556g	0.0254	0.0254	0.0506
Swing test	Result from Swing Test		0.0266	0.0266	0.0498
% Difference			− 4.5%	− 4.5%	1.6%

Table 9 Frequency domain average cost for RMAC with estimated inertia versus swing test

Flight condition	Swing test inertia	Geometry inertia	Difference
Hover	108	117	9
5 m/s	127	142	15

In the case of the multirotor vehicle, the geometry seems simple enough that approximations based on simplified geometry of the aircraft would be sufficiently close to the true. In practice, we found that simple approximations resulted in inertias that were within 5% of the swing test results, as shown in Table 8. Still, the average cost function of the physics-based model indicates that these small differences in inertia affect the overall model quality. The change in average cost shown in Table 9 is in the range considered significant, degrading the cost by $\Delta J = 9$ for hover and $\Delta J = 15$ for forward flight when using the approximate inertia. Clearly, to achieve excellent model accuracy, the inertias need to be very accurate and swing test results are warranted when practical.

8.4 Motor dynamics

As described earlier in Eqs. 2 and 3 , motor dynamics are included in the system identification model structure. As shown for a quadcopter [17] and for an octocopter [18], the inclusion of the motor dynamics are critical to accurately capturing higher frequency magnitude and phase response of multirotor vehicles. The pitch, roll and heave inputs are subject to a motor lag, as shown for example in the p/δ_{lat} model:

$$\frac{p}{\delta_{lat}} = \left(\frac{p}{\delta'_{lat}}\right)\left(\frac{\omega_{lag}}{s+\omega_{lag}}\right) \tag{18}$$

where p/δ'_{lat} is the response with instantaneous thrust (no motor lag). A similar structure is used for the pitch and thrust inputs. The yaw response is a combination of differential motor torques on alternating rotors, which produces a lead–lag motor dynamic:

$$\frac{r}{\delta_{yaw}} = \left(\frac{r}{\delta'_{yaw}}\right)\left(\frac{\omega_{lag}}{\omega_{lead}}\right)\left(\frac{s+\omega_{lead}}{s+\omega_{lag}}\right) \tag{19}$$

For the system ID model, these dynamics were identified as part of the model structure and it was determined that:

$\omega_{lag} = 15$ rad/s

$\omega_{lead} = 5.1$ rad/s

The RMAC physics-based model does not explicitly include these dynamics, which, if not corrected, results in an overprediction of phase at $\omega > 10$ rad/s. Considering that crossover frequency is expected to be in the range of $\omega \approx 15$ rad/s, this phase loss is exceedingly important for potential control system design. Overprediction of the phase will lead to an overprediction of phase margin, a dangerous situation that could result in flight instability. As such, the system identified first order motor dynamics were included in the RMAC physics-based model.

Modeling these motors explicitly would require knowledge of the electronic speed controller, motor and rotor inertia. These dynamics are most easily determined via system identification, an excellent example of system identification supplementing the physics-based model to improve its fidelity. In fact, these dynamics could be

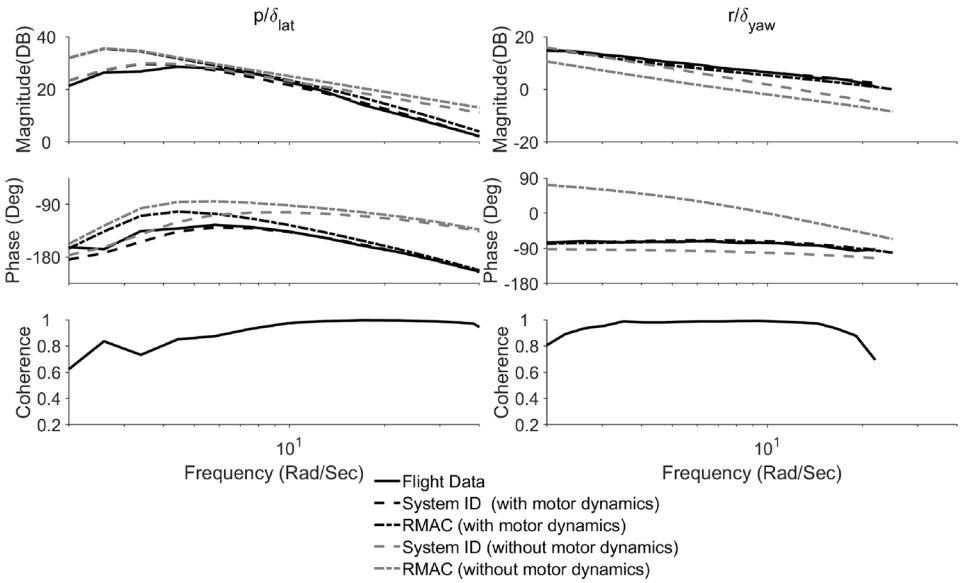

Fig. 22 Effect of motor dynamics on hover frequency responses

identified on a test stand as in [18] and then implemented prior to flight test to improve the physics-based model. Herein, we used the motor lag as identified in flight, because it was available.

As shown in Fig. 22, the inclusion of the motor dynamics is critical for the physics-based and system identification models. Both models tend to overpredict the gain and phase of the roll response at high frequency and underpredict the gain of the yaw response at high frequency (gray lines in Fig. 22). The RMAC model also greatly overpredicts the phase of the yaw response at all frequencies if motor dynamics are neglected.

8.5 Fuselage drag

Fuselage drag is a critical component of the dynamics of any VTOL aircraft, and multirotor aircraft are no exception. However, there are no first-principles models implemented in RMAC to estimate fuselage drag. Therefore, approximations of the fuselage drag must be made, ideally based on flight data. In this study, the fuselage flat plate drag area (0.0762 m^2) was chosen such that 5 m/s trimmed forward flight required approximately 6 degrees of nose-down pitch attitude. The flat plate drag area directly influences the predicted values of stability derivatives X_u and Y_v in forward flight. Figure 23 shows the pitch rate and longitudinal velocity rate responses to longitudinal input for varying levels of fuselage drag, ranging from zero to 100% increased drag. The amount fuselage drag does not significantly change the pitch rate responses, as expected, but the phase of the RMAC speed response $\dot{u}$ would be significantly over predicted if fuselage drag were ignored.

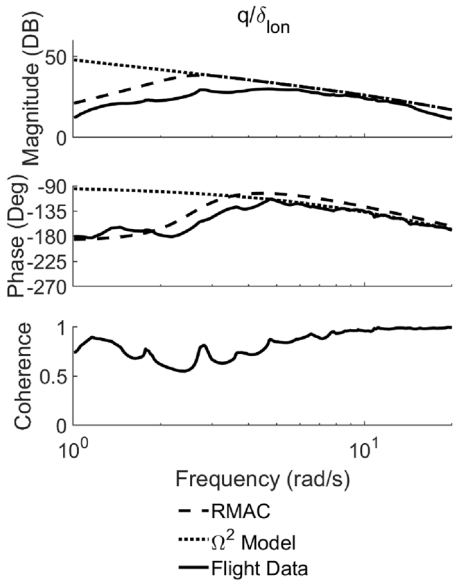

Fig. 24 Effect of rotor model on longitudinal dynamics in hover

8.6 Rotor modeling

In early quadcopter work [26, 27], rotor thrust and torque were calculated using a simple formula, with both being proportional to the square of the rotor rotational speed, with proportionality constants extracted from static thrust tests on the rotors used:

$$T = a\Omega^2 \tag{20}$$

$$Q = b\Omega^2 \tag{21}$$

Fig. 23 Effect of fuselage drag on predicted longitudinal dynamics

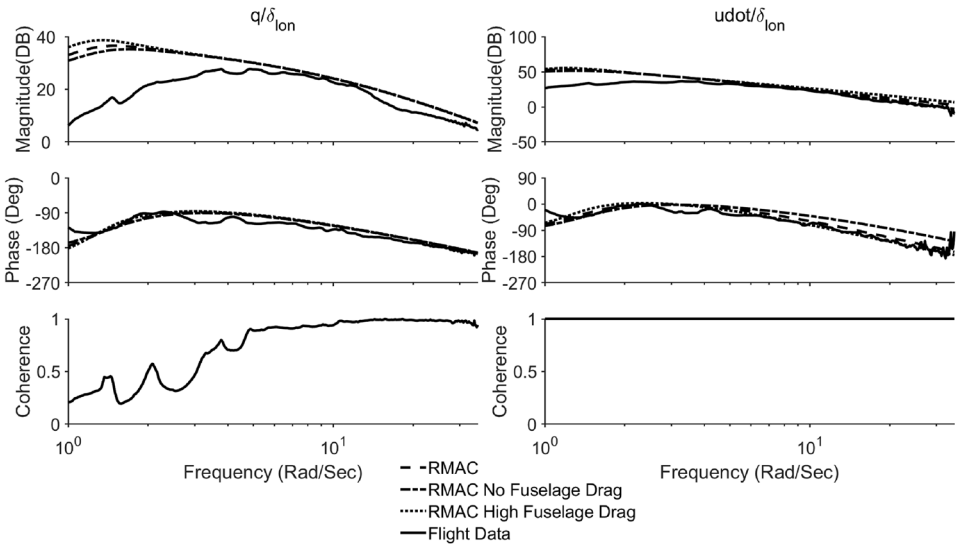

All other rotor forces and moments are assumed to be zero. The proportionality constants for thrust and torque were used throughout the flight envelope, with absolutely no adjustments based on the motion of the rotor relative to the surrounding air. Naturally, this model predicts control derivatives well in hover, but does not capture any of the stability derivatives that are associated with rotor forces or moments, such as M_u and L_v. Consequently, it does not capture well any of the low frequency bare airframe dynamics in hover or forward flight. For example, Fig. 24 shows the aircraft pitch rate response to longitudinal stick input. At high frequency, the Ω^2 model performs well, where the control derivative and motor dynamics (treated identically for Ω^2 as it is for RMAC in general) are dominant. However, at low frequency, the Ω^2 model dramatically overpredicts the magnitude of the pitch rate response, since it neglects the variation in inflow that occurs as the aircraft maneuvers.

9 Application of model corrections to physics-based model

The NATO Applied Vehicle Technology (AVT) 296 Research Task Group has examined several methods of model correction for the improvement of the fidelity of physics-based models using flight test data. The methods explored in the AVT-296 report [28] include:

1. Gain and time delay corrections
2. "Black-Box" input and output filters
3. Force and moment increments based on stability derivatives
4. Reduced order models and physics-based corrections
5. Model parameter adjustment for physics-based simulation
6. Parameter identification of key simulation constraints
7. Stitched simulations from point id models and trim data

Of these methods, both (1) and (2) have been applied to RMAC in earlier sections. Specifically, a time-delay correction from the identified data and an input filter representing the motor dynamics were added to the RMAC model. In this section, method (3), the force and moment increment will be applied to the RMAC model, in addition to the time delay and input filter corrections.

To correct the RMAC model with a force and moment increment using the identified hexacopter model, the first step is to identify which derivatives are important to get right, based on the sensitivity of the cost functions (Table 4) to changes in the individual stability and control derivatives. The corrections are made based on the model identified in hover, and the stability/control derivatives chosen for updates are summarized in Table 10.

Table 10 Selected derivatives for force and moment increment updates

Axis			
Longitudinal	Lateral	Heave	Yaw
X_u	Y_v	Z_w	None
M_u	L_v		
M_q	L_p		
$M_{\delta_{lon}}$	$L_{\delta_{lat}}$		

For the selected derivatives, an additional term is added to the equations of motion (Eqs. 7 and 8) to create Eqs. 22 and 23:

$$\begin{bmatrix}\dot{u}\\ \dot{v}\\ \dot{w}\end{bmatrix} = R^T\begin{bmatrix}0\\0\\g\end{bmatrix} + \frac{1}{m}\left(\mathbf{D}_{fus} + \sum_{i=1}^{6}\mathbf{F}_i + \begin{bmatrix}\Delta X\\ \Delta Y\\ \Delta Z\end{bmatrix}\right) - \boldsymbol{\omega}\times\mathbf{V} \tag{22}$$

$$\begin{bmatrix}\dot{p}\\ \dot{q}\\ \dot{r}\end{bmatrix} = \mathbf{I}^{-1}\left(\mathbf{r}_D\times\mathbf{D}_{fus} + \sum_{i=1}^{6}(\mathbf{M}_i + \mathbf{r}_i\times F_i) + \begin{bmatrix}\Delta L\\ \Delta M\\ \Delta N\end{bmatrix}\right) - \boldsymbol{\omega}\times\mathbf{I}\boldsymbol{\omega} \tag{23}$$

where ΔX, ΔY, ΔZ, ΔL, ΔM and ΔN are the force and moment increments, and are given by

$$\begin{aligned}
&\Delta X = (X_{u,ID} - X_{u,RMAC})u \qquad \Delta Y = (Y_{v,ID} - Y_{v,RMAC})v\\
&\Delta Z = (Z_{w,ID} - Z_{w,RMAC})w \qquad \Delta N = 0\\
&\Delta L = (L_{v,ID} - L_{v,RMAC})v + (L_{p,ID} - L_{p,RMAC})p\\
&\quad + (L_{\delta_{lat},ID} - L_{\delta_{lat},RMAC})\delta_{lat}\\
&\Delta M = (M_{u,ID} - M_{u,RMAC})u + (M_{q,ID} - M_{q,RMAC})q\\
&\quad + (M_{\delta_{lon},ID} - M_{\delta_{lon},RMAC})\delta_{lon}
\end{aligned} \tag{24}$$

The net effect of this change on the predicted stability and control derivatives are given by

Table 11 Frequency domain model validation costs (J) for corrected hover and forward flight models

Frequency response	Hover	5 m/s
a_x/δ_{lon}	100.3	92.3
$\dot{u}/\delta_{lon}$	85.7	50.7
q/δ_{lon}	66.6	35.6
a_y/δ_{lat}	129	68.7
$\dot{v}/\delta_{lat}$	71.9	33.8
p/δ_{lat}	60.1	31.4
r/δ_{yaw}	31.5	94.4
a_z/δ_{thr}	39.8	40.2
$\dot{w}/\delta_{thr}$	-	242
J_{ave}	73.1	76.56

$$A_{Corrected} = A_{RMAC} + (A_{hover,ID} - A_{hover,RMAC})$$
$$B_{Corrected} = B_{RMAC} + (B_{hover,ID} - B_{hover,RMAC}) \quad (25)$$

where only the derivatives in Table 10 are affected. Naturally, if A_{RMAC} and B_{RMAC} are evaluated in hover, the selected stability derivatives will match the identified model, bringing the frequency responses much closer to the identified models, as shown by the reduced costs listed in Table 11. The costs are not quite identical to the identified model, as only a subset of stability derivatives have been updated.

When the same correction is applied to the forward flight model, all of the model costs are reduced dramatically. In fact, all of the on-axis model costs are within the guideline of $J < 100$, except for $\dot{w}/\delta_{thr}$. This frequency response is still largely incorrect due to the errors in M_w, as previously described. This stability derivative was not selected for correction, as it is equal to zero in hover.

If Eq. 25 is applied about 5m/s instead of hover, then even the coupled responses would be accurately predicted. However, this would also result in a pitch-heave coupling in hover, which is not observed in the flight data. As such, a multi-point correction may be necessary to accurately capture the behavior in both hover and forward flight.

10 Conclusions

This paper performed a detailed evaluation of the predictive capabilities of system identification using CIFER® and a physics-based nonlinear blade-element model with 10 state Peters-He inflow as implemented in the Rensselaer Multicopter Analysis Code (RMAC). The models were validated against flight data in both the time and frequency domains for a 55 cm diameter hexacopter at hover and forward flight (5 m/s). Model corrections using the force and moment increments from the identified model were applied to the RMAC model. Key conclusions from this work are given below.

System identification model

1. Frequency domain system identification models are highly accurate at both hover and forward flight for multirotor vehicles, resulting models that produce nearly identical responses as flight.
2. Speed damping derivatives L_v and M_u, which largely dominate the roll and pitch dynamics at hover, are somewhat reduced at forward flight, whereas pitch and roll damping (L_p and M_q) play a larger role in forward flight
3. Coupling between pitch and heave becomes more prevalent in forward flight, where $M_{\delta_{thr}}$ and M_w derivatives are identified with non-zero values.
4. Motor lag and time delay are constant across both flight conditions and are critical for accurate system identification.

Physics-based blade element RMAC model

5. The inertia of the vehicle must be very accurate for a good prediction of the flight response. Mass moment of inertia determined by swing test of the hexacopter provided significant improvement in the RMAC prediction.
6. The motor lag and time delay dynamics are important elements of the high frequency phase response of the vehicle, and must be accounted for the physics-based model. An empirical first-order model from system identification results was found sufficient to model these key dynamics.
7. RMAC model under-predicts the speed derivatives (L_v, M_u) and over-predicts the rate damping derivatives (L_p, M_q), resulting in poor predictive accuracy at low frequency ($\omega < 5$). In addition, in forward flight, the pitch response due to coupling with heave is significantly overpredicted.
8. RMAC model has sufficient accuracy in the frequency range of interest for flight control to support preliminary design.

Model corrections

9. Applying the force and moment increment to a subset of stability derivatives in hover reduced the model cost dramatically in hover.
10. Applying the same increment identified in hover to the forward flight model dramatically reduced the model cost for most of the on-axis frequency responses. The sole exception was the heave response, which is influenced by the overpredicted pitch-heave coupling. This was not corrected, as the coupling derivatives are zero in hover.
11. To accurately capture the behavior in hover and forward flight, a multi-point correction method may be necessary.

Acknowledgements This paper is an extension of the work that was previously presented at the 75th Annual Forum of the Vertical Flight Society as "Multirotor Electric Aerial Vehicle Model Validation with Flight Data: Physics-Based and System Identification Models." The work has been expanded to include model corrections for the physics-based model.

Funding This work is carried out at Rensselaer Polytechnic Institute under the Army/ Navy/NASA Vertical Lift Research Center of Excellence (VLRCOE) Program, grant number W911W61120012, with Dr. Mahendra Bhagwat as Technical Monitor.

Availability of data and materials The simulation data used in this study is available upon request.

Code availability The code used for simulation is not available.

Declarations

Conflict of interest Not Applicable

Previous Publication This work was presented at the 75th Annual Forum of the Vertical Flight Society as "*Multirotor Electric Aerial Vehicle Model Validation with Flight Data: Physics-Based and System Identification Models*." The work has been expanded to include model corrections for the physics-based model.

References

1. FAA, FAA Forecasts Fiscal Years 2018–2038, (2018)
2. Patterson, M., Antcliff, K., Kohlman, L.: A Proposed Approach to Studying Urban Air Mobility Missions Including an Initial Exploration of Mission Requirements, Proceedings of the 74th AHD International 74th Annual Forum, Phoenix, AZ, (2018)
3. Gettinger, D., Michel, A. H.: Drone Sightings and Close Encounters: An Analysis, Technical report, Center for the Study of the Drone, Bard College, Annandale-on-Hudson, New York, (2015)
4. Klyde, D., Mitchell, D., Alexandrov, N.: Development of a Process to Define Unmanned Aircraft Systems Handling Qualities, AIAA Atmospheric Flight Mechanics Conference, Kissimmee, FL, (2018)
5. Maskel, R., D.A.S.H.: Goes to War, Air & Space Smithsonian, https://www.airspacemag.com/military-aviation/dash-goes-to-war-23369442/, (2012)
6. Colbourne, J., Tischler, M., Rodgers, K.: Flight Control Design for an Unmanned Rotorcraft Program with a Rapid Development Schedule, Proceedings of the American Helicopter Society 57th Annual Forum, Washington, D.C., (2001)
7. Colbourne, J., Frost, C., Tischler, M., Tomashofki, R. C., LaMontagne, T.: System Identification and Control Design for the BURRO Autonomous UAV, Proceedings of the American Helicopter Society 56th Annual Forum, Virginia Beach, VA, (2000)
8. Mettler, B., Tischler, M., Kanade, T.: System Identification of Small-Sized Unmanned Helicopter Dynamics, Proceedings of the American Helicopter Society 55th Annual Forum, Montreal, Quebec, Canada, (1999)
9. Kim, S.K., Tilbury, D.M.: Mathematical Modeling and Experimental Validation of Unmanned Helicopter Robot with Fly Bar Dynamics. J. Robotic Syst. **21**(3), 95–116 (2004)
10. Theodore, C., Tischler, M., Colbourne, J.: Rapid Frequency Domain Modeling Methods for UAV Flight Control Applications, AIAA Atmospheric Flight Mechanics Conference and Exhibit, Austin, TX, (2003)
11. Quidling, C., Ivler, C., Tischler, M.: GenHel S-76C Model Correlation using Flight Test Identified Models, Porceedings of the American Helicopter Society International 64th Annual Forum. Montreal, Quebec, Canada (2008)
12. Tobias, E., Tischler, M., Sanders, F.: Full-Envelope Stitched Simulation Model of a Quadcopter using STITCH, Proceedings of the American Helicopter Society International 74th Annual Forum, Phoenix, AZ, (2018)
13. Ivler, C., Tischler, M.: Case Studies of System Identification Modeling for Flight Control Design. J. Am. Helicopter Soc. **58**(1), 1–16 (2013)
14. Fegely, C., Juhasz, O., Xin, H., Tischler, M.: Flight Dynamics and Control Modeling with System Identification Validation of the Sikorsky X2 Technology Demonstrator, Proceedings of the American Helicopter Society International 72nd Annual Forum, West Palm Beach, FL, (2016)
15. Tischler, M., Remple, R.: Aircraft and Rotorcraft system Identification: Engineering Methods with Fligh Test Examples, AIAA Education Series, second edition, (2012)
16. Wei, W., Cohen, K., Tischler, M.: System Identification and Controller Optimization of a Quadrotor UAV, Proceedings of the American Helicopter Society International 71st Annual Forum, Virginia Beach, VA, (2015)
17. Cheung, K., Wagner, J., Tischler, M., Ivler, C., Berrios, M., Berger, T., Juhasz, O., Tobias, E., Goerzen, C., Barons, P., Sanders, F., Lopez, M., and Lehmann, R.: An Overview of the U.S. Army Aviation Development Directorate Quadrotor Guidance, Navigation, and Control Project, Proceedings of the American Helicopter Society International 73rd Annual Forum, Fort Worth, TX, (2017)
18. Gong, A., Sanders, F., Hess, R., Tischler, M.: System Identification and Full Flight Envelope Model Stitching of a Package-Delivery Octocopter, Proceedings of the AIAA SciTech Forum, San Diego, CA, (2019)
19. Lopez, M., Tischler, M., Juhasz, O., Gong, A., Sanders, F.: Development of a Reconfigurable Multicopter Flight Dynamics Model From Flight Data using System Identification, Proceedings of the Vertical Flight Society Autonomous VTOL Technical Meeting, Mesa, AZ, (2019)
20. Niemiec, R., Gandhi, F.: Development and Validation of the Rensselaer Multicopter Analysis Code (RMAC): A Physics-Based Comprehensive Modeling Tool, Proceedings of the Vertical Flight Society 75th Annual Forum, Philadelphia, PA, (2019)
21. ardupilot.org, [Online], Available: www.ardupilot.org [Accessed 7-4-2019]
22. Ivler, C., Rowe, E., Martin, J., Tischler, M.: System Identification Guidance for Multirotor Aircraft: Dynamics Scaling and Test Techniques, Proceedings of the Vertical Flight Society 75th Annual Forum, Philadelphia, PA, (2019)
23. Niemiec, R., Gandhi, F.: Effect of Inflow Model on Simulated Aeromechanics of a Quadrotor Helicopter, Proceedings of the 72nd Vertical Flight Society Annual Forum, West Palm Beach, FL, (2016)
24. Peters, D., Boyd, D.D., He, C.: Finite-State Induced-Flow Model for Rotors in Hover and Forward Flight. J. Am. Helicopter Soc. **34**(4), 5–17 (1989)
25. Niemiec, R., Gandhi, F.: Multi-Rotor Coordinate Transform for Orthogonal Primary and Redundant Control Modes for Regular Multicopters, 42nd European Rotorcraft Forum. Lille, France (2016)
26. Bouabdallah, S., Seigwart, R.: Design and Control of a Quadcopter, Proceedings of the 2004 IEEE International Conference on Robotics and Automation, Picastaway, NJ, (2004)
27. Mueller, M., D'Andrea, R.: Stability and Control of a Quadcopter Despite the Complete Loss of One, Two, or Three Propellers, Proceedings of the 2007 IEEE International Conference on Robotics and Automation, Picastaway, NJ, (2007)
28. NATO.: Rotorcraft Flight Simulation Model Fidelity Improvement and Assessment, Technical Report STO-TR-AVT-296-UU, (2021)